SYNCHROTRON RADIATION IMPACT ON THE FCC-ee ARCS

B. Humann*[1], F. Cerutti, R. Kersevan, CERN, Geneva, Switzerland

[1]also at TU Wien, Vienna, Austria

Abstract

Synchrotron radiation (SR) emitted by electron and positron beams represents a major loss source in high energy circular colliders, such as the lepton version of the Future Circular Collider (FCC-ee) at CERN. In particular, for the operation mode at 182.5 GeV (above the top pair threshold), its spectrum makes it penetrate well beyond the vacuum chamber walls. In order to optimize its containment, dedicated absorbers are envisaged. In this contribution we report the energy deposition studies performed with FLUKA to assess heat load, time-integrated dose and particle fluence distribution in the machine components and the surrounding environment. Different choices for the absorber material were considered and shielding options for electronics were investigated. Furthermore, possible positions for the booster ring were reviewed from the radiation exposure point of view.

INTRODUCTION

The lepton machine of Future Circular Collider (FCC-ee) is one option for a future accelerator at CERN. With a circumference of around 91 km, it is meant to collide electrons and positrons at four different energies ranging from 45.6 GeV (Z mode) to 182.5 GeV (ttbar mode) [1]. In a lepton machine, synchrotron radiation (SR) is a major source of beam energy loss impacting the accelerator. Therefore, it is necessary to assess its effects on the magnets and the tunnel environment. These studies are performed with FLUKA [2–4], a Monte Carlo particle transport and interaction code, with which the energy deposition caused by the SR in the FCC-ee collider arcs was simulated.

SR is electromagnetic radiation emitted tangentially by charged particles that follow a curved trajectory. The energy loss per turn, ΔE, is given as

$$\Delta E = \frac{e^2}{3\varepsilon_0(m_0c^2)^4}\frac{E^4}{\rho},\qquad(1)$$

indicating the high impact of SR in electron and positron colliders due to the small rest mass, m_0, of these particles. In Eq. 1, e is the elementary electric charge, ε_0 the vacuum permittivity, E the energy of the circulating particles and ρ is the bending radius, equal to 10.76 km for the FCC-ee machine [5]. This leads to $\Delta E_{182.5\,\text{GeV}} = 9.2\,\text{GeV/turn}$ and $\Delta E_{45.6\,\text{GeV}} = 0.036\,\text{GeV/turn}$. The critical energy E_C is defined as splitting the emitted photon spectrum in two equal parts in terms of integrated power [6]. Its expression

$$E_C = \frac{3}{2}\hbar c\frac{\gamma^3}{\rho} \approx 2.21 \cdot 10^{-6}\frac{E^3[GeV]}{\rho[km]}[MeV]\qquad(2)$$

yields $E_C^{182.5\,\text{GeV}} = 1.25\,\text{MeV}$, being γ the relativistic Lorentz factor. For the operation mode at 45.6 GeV, where the energy is a factor 4 lower, the critical energy is $E_C^{45.6\,\text{GeV}} = 19\,\text{keV}$. Figure 1 shows the SR photon spectra for the two extreme energies of colliding beams in FCC-ee, emphasising the very different penetration capacity of the emitted radiation, which in the Z mode is fully absorbed by the vacuum chamber walls.
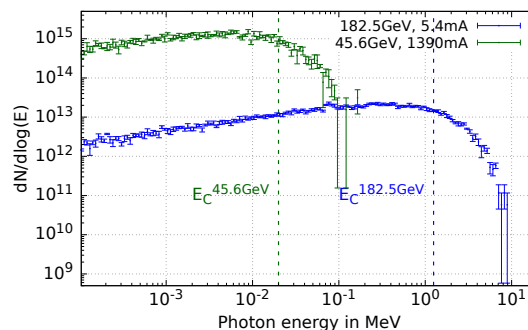

Figure 1: SR spectra for the 45.6 GeV and 182.5 GeV FCC-ee operation modes, as generated by FLUKA. Their integral gives the amount of photons emitted by the electron/positron beam over 1 cm.

By design, the SR power shall be constant for all operation modes and amount to 50 MW per beam. This implies a current of 5.4 mA for the highest operation energy and 1390 mA for the lowest one.

SIMULATION SETUP

For this study, a representative 140 m long periodic cell of the FCC-ee arc was simulated, as displayed in Fig. 2. It consists of 5 dipoles (MB), 5 quadrupoles (MQ) and 4 sextupoles (MS), that are held at room temperature. Two dipoles have a length of 21 m and the other three are 24 m long. The MQs have a length of 3 m and the MSs, that are placed in pairs before the first two MQs (according to the clockwise direction), have a length of 1.3 m. The MB and MQ geometries are based on the technical drawings of the already existing prototypes [1], while the MS model was extracted from an early stage sketch.

Three different SR shielding options are investigated. The main focus is on the shielding performed with dedicated photon absorbers. In total, 25 absorbers per beam with a length of 30 cm each are placed every 5-6 m inside the MB and MQ vacuum chamber, in order to prevent the latter from being directly impacted by the SR. They are made of a CuCrZr alloy, which has good absorption and mechanical properties. In the following, they are referred to as "copper absorbers". As an alternative, absorbers made out of a tungsten alloy
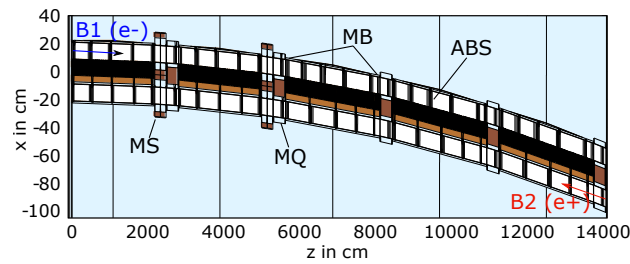
* barbara.humann@cern.ch

Figure 2: Top view of the arc cell, displaying the magnets at beam level and the circulating beams (B1...beam 1, B2...beam 2).

(Inermet 180®), that offers better absorption properties but has a higher cost, are considered. For comparison, a continuous tungsten alloy shielding, inspired by the lead one of the former LEP accelerator pipe, is studied [7]. Due to lack of space inside the MQs and MSs, it is only implemented in the MBs. The accelerator structure is embedded in a realistic tunnel geometry (see Fig. 3) [1].
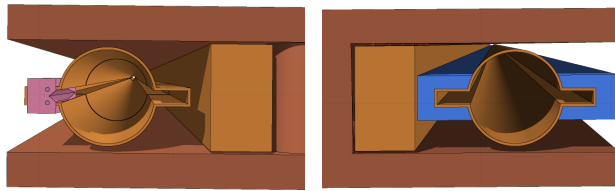

Figure 3: Localized absorber (on the left) and continuous shielding (on the right) in a dipole.

For each accelerator component, the thermal load is assessed. Moreover, the distribution of the accumulated ionising dose is calculated to estimate long term radiation effects such as material degradation. This is not critical for the FCC-ee arc warm dipoles, because their coils do not contain any organic insulator. On the other hand, it plays an important role to define the electronics equipment lifetime. In this regard, also Si-1 MeV neutron equivalent fluence, thermal neutron equivalent fluence and high energy hadron equivalent fluence are relevant quantities, that are used to anticipate cumulative and stochastic damage in electronics [8]. In the following, the ttbar mode current of 5.4 mA is used for normalization. Time integrated results refer to one year of operation which is assumed to be 1×10^7 s.

SIMULATION RESULTS

Power Deposition on the Accelerator Components

Over the considered 140 m long arc cell, the SR emitted by the two circulating beams deposits 167 kW. Comparing the layouts with absorbers and continuous shielding, a different sharing is obtained, as detailed in Table 1.

The same amount of power goes onto the continuous tungsten shielding and the copper absorbers, while the tungsten absorbers get about 15% more. On average, this corresponds to 2.6 kW per copper absorber and 3.1 kW per tungsten ab-

Table 1: Absorbed power per element type for the different absorber (ABS) layouts and the continuous shielding (Shield)

	Tungsten	Copper	Continuous
ABS or Shield	155 kW	131 kW	135 kW
MB	7.8 kW	23.4 kW	3.5 kW
MQ	0.9 kW	2.6 kW	17.4 kW
MS	0.05 kW	0.09 kW	7.1 kW
Tunnel	4.1 kW	9.5 kW	3.5 kW
Total	**167 kW**	**167 kW**	**167 kW**

sorber. There is a significant difference for the magnets, with better protected dipoles in the case of continuous shielding and tungsten absorbers. On the other hand, for the quadrupoles and sextupoles the absorbed power is much higher for the case of continuous shielding, due to its interruption inside them. The tunnel walls are more impacted in the copper case, by a factor 2.5. Finally, the vacuum chambers take 10 W/m in the absorber cases and more than 350 W/m for the continuous shielding, which highlights a major challenge for the latter option.

Long Term Radiation Effects

Radiation levels in the tunnel affect layout and infrastructure choices that have to be finalised within the next 20 years. Three-dimensional dose maps were calculated over the whole tunnel volume and Table 2 reports reference values in air at beam height and one metre above. For the absorber cases, on the machine plane a higher dose is observed inside the ring, due to the SR photon reflection by the internal beam absorbers. As for the particles reflected by the external beam absorbers, they are intercepted by the double-C shaped structure of the dipoles. As previously indicated by integral power results, the tungsten absorbers assure a reduced leakage. Nevertheless, the continuous shielding yields here the lowest dose values here, with the noticeable exception of 1.2 MGy peaks in correspondence of the MQs, where no shielding is implemented.

Table 2: Annual dose levels in the tunnel for the different absorber schemes. For the beam level, data for the external (ext.) and internal (int.) side of the ring is given.

	Tungsten	Copper	Continuous
Beam level, ext.	100 kGy	600 kGy	200 kGy
Beam level, int.	500 kGy	1 MGy	200 kGy
Above beam	100 kGy	300 kGy	120 kGy

The picture changes above the collider. There the dose is more homogeneously distributed in both absorber cases, with higher values found again for the copper case. With the continuous shielding, one gets 120 kGy per year, but at the locations of the MQs, featuring larger doses for the same reason as before.

These results confirm that the ideal placement of the booster ring is above the collider due to the lower dose levels. For the electronic equipment, the reported dose levels are by far too high. For comparison, annual values of few Gy are expected in the LHC arcs after the High Luminosity (HL) upgrade [9]. Hence, a dedicated shielding has to be elaborated, as discussed in the next section.

While the dose levels are rather different for the three SR shielding options, the estimates of Si-1 MeV neutron equivalent fluence, associated to the cumulative damage to electronics by non-ionising energy losses, are similar. They give about 2×10^{12} cm^{-2} per year, which is two orders of magnitude higher than the HL-LHC reference value. It has to be noted that for the different absorber materials, different relative contributions by neutrons and electromagnetic particles are observed. Tungsten has a lower neutron production threshold for photo-nuclear reactions as well as a higher absorption power for electromagnetic particles, which means that in this case, the neutron contribution to the Si-1 MeV neutron equivalent fluence in the tunnel is not negligible. With copper absorbers, as a consequence of the higher photo-neutron production threshold, the electromagnetic contribution is by far dominant, despite the much lower efficiency of electrons and positrons in inducing atom displacements, which is compensated by their high abundance.
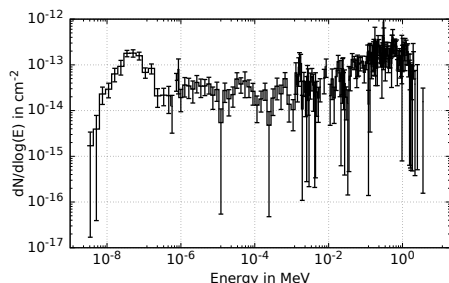

Figure 4: Annual neutron fluence spectrum with statistical error in the tunnel volume. The thermal peak is visible on the left.

The thermal neutron equivalent fluence is similar in all three cases and is of the order of 2×10^{11} cm^{-2} per year. The high energy hadron equivalent fluence drops to 2×10^{8} cm^{-2} per year, one order of magnitude less than in the HL-LHC arcs, since the neutron spectrum hardly exceeds a few MeV in the FCC-ee, as seen in Fig. 4.

ELECTRONICS SHIELDING SCHEME

As mentioned above, standard electronics cannot withstand the expected dose levels in the FCC-ee tunnel, even with the various measures for SR absorption put in place. To address this problem, specific shielding layouts are investigated. They are located in the bottom external corner of the tunnel, where the dose distribution decreases. Continuous concrete or lead walls of different thickness (1 cm, 3 cm and 10 cm) are tested for the copper absorber case that leads to the worst dose scenario in the tunnel (see Table 2).

Behind a 10 cm concrete shielding, the dose is reduced to a value roughly similar to the one achieved with a 3 cm lead layer, namely 50 kGy. The feasibility of a significantly thicker lead layer, potentially assuring not to exceed 1 kGy, requires further follow-up. In fact, a 10 cm lead layer would also reduce by two orders of magnitude the Si-1 MeV neutron equivalent fluence, being particular effective for the electromagnetic component that dominates this quantity, as earlier discussed. On the other hand, the attenuation of the neutron component, ruling high energy hadron equivalent fluence and thermal neutron equivalent fluence values, calls for a shielding optimization by means of an external layer of borated polyethylene. This slows the neutrons down and captures them, with the lead layer absorbing secondary gamma rays.

While the absence of the additional layer leaves the neutron spectrum almost unaltered through the relatively thin concrete and lead layers, Figure 5 shows the evolution of the photon spectrum from the tunnel air volume through the lead layer down to the shielded area ideally reserved for electronics, where a marked attenuation can be appreciated as a function of the lead thickness.
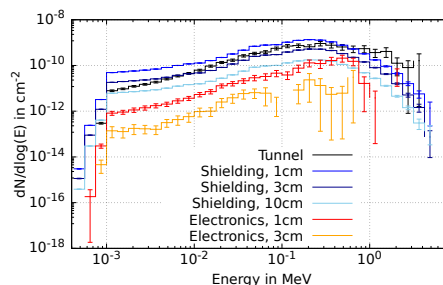

Figure 5: Photon fluence spectra with statistical error in the indicated regions of the FCC-ee arc tunnel for different lead shielding thicknesses, referring to the copper absorber layout. No curve is given in the electronic equipment region for the 10 cm case, due to poor statistics.

CONCLUSION

Energy deposition studies to assess the effects of SR in the FCC-ee arc were performed with FLUKA. Three different SR shielding options were tested. Two of them are based on localized absorbers made out of CuCrZr and Inermet180®, and the third option is a continuous shielding attached to the winglets of the dipole vacuum chambers. Each of the copper absorbers catches on average 2.6 kW, rising to 3.1 kW for the tungsten ones. The dose levels on the beam plane are up to a factor 2 to 5 higher than above the collider, therefore the placement of the booster machine on top is preferable. Standard electronics cannot withstand the radiation levels in the tunnel, so a preliminary scheme for a dedicated shielding was studied, quantifying its mitigation margins.

ACKNOWLEDGEMENTS

MC1: Circular and Linear Colliders

A02: Lepton Colliders

REFERENCES

[1] M. Benedikt et al., "Future Circular Collider Study. Volume 2: The Lepton Collider (FCC-ee) Conceptual Design Report," CERN, Geneva, accelerator reports CERN-ACC-2018-0057, Dec. 2018, Published in Eur. Phys. J. ST.

[2] CERN, *FLUKA Website*, https://fluka.cern.

[3] C. Ahdida et al., "New Capabilities of the FLUKA Multi-Purpose Code," *Frontiers in Physics*, vol. 9, 2022. doi:10.3389/fphy.2021.788253. https://www.frontiersin.org/article/10.3389/fphy.2021

[4] G. Battistoni et al., "Overview of the FLUKA code," *Ann. Nucl. Energy*, vol. 82, 10–18. 9 p, 2015. doi:10.1016/j.anucene.2014.11.007. http://cds.cern.ch/record/2162467

[5] K. Wille, *Synchrotron Radiation*, JUAS 2013, accessed 13/05/2022, 2013. https://indico.cern.ch/event/218284/contributions/1520454/attachments/352184/490697/JUAS2013_Synchrotron_Radiation_1pdf

[6] R. Bartolini, *Synchrotron Radiation*, JUAS 2017 - Week 4, accessed 13/05/2022, 2017. https://indico.cern.ch/event/569714/contributions/2303963/attachments/1336452/2143086/JUAS_2017_RB_synchrotron_radiation_I.pdf

[7] G. Chapman et al., "Synchrotron Radiation Lead Shielding of the Vacuum Chambers for LEP," *IEEE Transactions on Nuclear Science*, vol. 30, no. 4, pp. 2340–2342, 1983. doi:10.1109/TNS.1983.4332809

[8] R. García Alía, "Radiation Fields in High Energy Accelerators and their impact on Single Event Effects. Champs ionisants dans un accélérateur à haute énergie et leur impact sur les Effets Singuliers," Presented 15 Dec 2014, Oct. 2014. https://cds.cern.ch/record/2012360

[9] G. Lerner et al., *RADIATION LEVEL SPECIFICATIONS FOR HL-LHC*, EDMS NO. 2302154 v1.0, accessed 13/05/2022, 2020. https://edms.cern.ch/ui/file/2302154/1.0/HLLHC_Specification_Document_v1.0.pdf